Lattice and magnetic instabilities in $Cu_3Bi(SeO_3)_2O_2X$ (X = Br, Cl)

V. Gnezdilov,[1,2] Yu. Pashkevich,[3] P. Lemmens,[1] V. Kurnosov,[2] P. Berdonosov,[4] V. Dolgikh,[4] E. Kuznetsova,[4] V. Pryadun,[4] K. Zakharov,[4] and A. Vasiliev[4,5,6]

[1]*Institute of Condensed Matter Physics, TU Braunschweig, D-38106 Braunschweig, Germany*
[2]*Institute for Low Temperature Physics and Engineering NASU, 61103 Kharkov, Ukraine*
[3]*Donetsk Institute for Physics and Engineering NASU, 03680 Kiev, Ukraine*
[4]*Lomonosov Moscow State University, 119991 Moscow, Russia*
[5]*National University of Science and Technology "MISiS", 119049 Moscow, Russia*
[6]*National Research South Ural State University, 454080 Chelyabinsk, Russia*

(Received 17 April 2016; revised manuscript received 24 July 2017; published 21 September 2017)

Specific heat C, thermal conductivity κ, dielectric permittivity ε, electric polarization P, and Raman scattering experiments are performed on $Cu_3Bi(SeO_3)_2O_2X$ (X = Br, Cl) single crystals. The Cl compound undergoes a structural phase transition at $T^* \sim 115$ K evident in $C(T)$, $\varepsilon(T)$, and $\kappa(T)$ and accompanied by the appearance of unique phonon lines in Raman scattering. No evident structural changes are detected in the Br compound. At $T < T^*$, a very weak polarization loop with a $P \parallel c$ axis is observed in the Cl compound. Both compounds order antiferromagnetically at comparable temperatures $T_N \sim 25$ K marked by sharp λ-type singularities. For $T < T_N$, an intensive mode of magnetic origin appears in both compounds. At the lowest temperatures, the energy of this mode is in good agreement with both the magnon excitation observed in infrared spectroscopy and the spin gap found recently in inelastic neutron scattering of the Cl compound.

DOI: 10.1103/PhysRevB.96.115144

I. INTRODUCTION

Both title species of francisite-type compounds, $Cu_3Bi(SeO_3)_2O_2X$ (X = Br, Cl), have recently been in the focus of hot discussions regarding the interplay of their crystal structure, and electric and magnetic properties [1–4]. The recent observation of field-induced type II multiferroicity at a metamagnetic phase transition just poured oil on the flames [5]. Apart from academic interest, the controllable broadband absorption of microwaves exhibited by these materials has attracted vivid attention due to several promising applications of this phenomenon [6,7].

In the broader context, the Bi-based francisites belong to a versatile family of $Cu_3R(ChO_3)_2O_2X$ compounds, where R stands for Bi, Y, and rare earth; the position of chalcogen Ch can be occupied by Se and Te; and the halogen X position may belong to Cl, Br, and I [8–10]. All these compounds adopt layered buckled kagome structure with halogen ions being weakly coupled within interlayer hexagonal tunnels [11]. At low temperatures, the francisites stabilize exotic canted antiferromagnetic order with Néel temperature T_N ranging from 24 K in $Cu_3Bi(SeO_3)_2O_2Cl$ to 43 K in $Cu_3Dy(SeO_3)_2O_2Cl$. The simultaneous presence of magnetically active divalent copper and lone pair elements, bismuth and selenium, in pristine francisite, $Cu_3Bi(SeO_3)_2O_2Cl$, ensures very rich physics in different experimental probes [12–18]. The appearance of rare-earth elements in the francisite structure leads to further complications in magnetic response of these materials caused by strong interaction of the rare earth and transition-metal subsystems. In some cases, the spin-reorientation transition of either first [in $Cu_3Yb(SeO_3)_2O_2Cl$] or second [in $Cu_3Sm(SeO_3)_2O_2Cl$] order occurs at $T < T_N$ [19].

Among every known member of the francisite family only the chlorine compound exhibits a structural phase transition at $T^* = 115$ K far above the magnetic ordering temperature $T_N = 24$ K [12]. While there is a consensus regarding parent centrosymmetric $Pmmn$ crystal structure of both the Br compound and the high-temperature phase of the Cl compound [9,20], several candidates were considered for the structure of the low-temperature phase of Cl francisite. Basing on infrared and preliminary Raman measurements [12] it was conjectured that the low-temperature structure of $Cu_3Bi(SeO_3)_2O_2Cl$ belongs to the polar ferroelectric $P2_1mn$ space group. Attempts were made to analyze the single-crystal neutron diffraction data in both $Pcmn$ and polar ferroelectric $Pc2_1m$ space groups; preference has been given to the former [4]. Finally, the high-resolution synchrotron powder diffraction measurements identified the low-temperature structure as the nonpolar antiferroelectric $Pcmn$ phase with a small (about 10%) admixture of $P2_1mn$ phase [3]. The simultaneous formation of these two phases in $Cu_3Bi(SeO_3)_2O_2Cl$ dependent on the pattern of Cl and Cu2 displacements can be represented by the structure shown in Fig. 1, where the splitting of Cl and Cu2 positions is marked by sectoral circles. It should be noted, however, that the analysis of the fractional occupancy of the Cl position, given in Ref. [3], supports an alternative explanation of x-ray diffraction data concerning residual disorder of the halogen in $Pcmn$ structure. Moreover, it is claimed that even better structure refinement at 200 K was obtained using the disordered $Pcmn$ model instead of the $Pmmn$ model.

The canted magnetic structure in francisites has been established initially in single-crystal neutron diffraction measurements on $Cu_3Bi(SeO_3)_2O_2Br$ [14]. Below $T_N = 27$ K, this compound exhibits an alternating antiferromagnetic order of the ab kagome layers with canted ferrimagnetic arrangement of individual copper moments within each layer. With an external magnetic field $B \leqslant 1$ T oriented along the c axis, a metamagnetic transition occurs through a turnover of every second ab layer resulting in an overall ferrimagnetic noncollinear spin arrangement. The presence of a canted antiferromagnetic structure in francisite-type compounds in the absence of an external magnetic field is further confirmed by powder

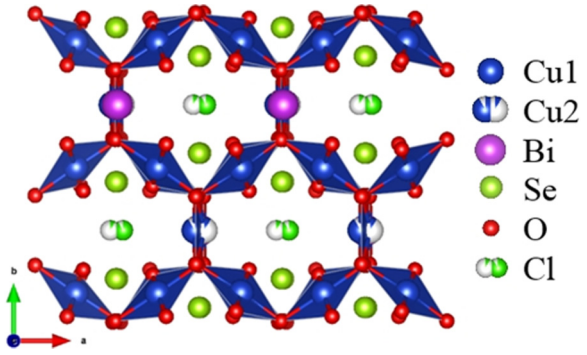

FIG. 1. The *ab* projection of low-temperature crystal structure of $Cu_3Bi(SeO_3)_2O_2Cl$ as generated from the francisite-Cl-10K.cif file in the supplemental material of Ref. [3].

neutron diffraction measurements on $Cu_3Y(SeO_3)_2O_2Cl$ [17]. Recently, a canted magnetic structure was identified in $Cu_3Bi(SeO_3)_2O_2Cl$ through single-crystal neutron diffraction, the only difference being that the canting angle was found to be 59° as opposed to 50° in $Cu_3Bi(SeO_3)_2O_2Br$ [4]. Overall, the magnetic properties, similar to those found in the pristine compound, were found in static magnetization measurements in every francisite, $Cu_3R(ChO_3)_2O_2X$, studied so far [15,16].

First-principles electronic structure calculations show that the canted magnetic moments in francisites arise from a competition of ferromagnetic Cu-O-Cu nearest-neighbor and antiferromagnetic Cu-O-O-Cu next-nearest-neighbor exchange interactions within kagome layers, while weaker anisotropic terms define the spin directions with respect to crystallographic axes [1,2]. The spin gap of about $35\,cm^{-1}$, an important feature of spin excitation spectra in $Cu_3Bi(SeO_3)_2O_2Cl$, not considered in the initially suggested models demands a sizable symmetric exchange anisotropy beyond the proposed Dzyaloshinskii-Moriya interaction [4].

Regarding the dielectric subsystem, there is less agreement between theory and experimental observations. As follows from density-functional calculations of ground-state energy, the nonpolar antiferroelectric structure *Pcmn* of the low-temperature phase of $Cu_3Bi(SeO_3)_2O_2Cl$ is only slightly lower in energy than the polar $P2_1mn$ structure, but no convincing evidence of its formation could be obtained [3]. The structural phase transition in $Cu_3Bi(SeO_3)_2O_2Cl$ is marked by weak anomaly in dielectric permittivity at $T^* = 115\,K$ [5]. The appearance of a spontaneous electric polarization was detected for $T \leqslant T^*$ [4]. It switches polarity at the application of positive and negative poling electric fields in the range $T_N \leqslant T \leqslant T^*$. At the same time, the polarization below T_N was found to be unaffected by poling fields. Finally, the magnetic-field-induced ferroelectric behavior was observed in $Cu_3Bi(SeO_3)_2O_2Cl$ at metamagnetic phase transition in a magnetic field $B \parallel c$ axis [5].

In this work, we performed detailed Raman spectroscopy studies of the temperature dependences of vibrational and magnetic excitations in $Cu_3Bi(SeO_3)_2O_2X$ (X = Cl, Br) accompanied by measurements of specific heat C, thermal conductivity κ, dielectric permittivity ε, and electric polarization P.

II. EXPERIMENTAL DETAILS

A. Methods

The bright green platelike single crystals of $Cu_3Bi(SeO_3)_2O_2X$ (X = Br, Cl) with the c axis oriented along the surface normal were grown by the chemical vapor transport method and characterized by powder x-ray diffraction at room temperature (the details are given in the Supplemental Material [21]). The patterns were indexed in the space group *Pmmn* with cell constants for $Cu_3Bi(SeO_3)_2O_2Cl$ $a = 6.341(5)$, $b = 9.641(10)$, and $c = 7.222(6)$ Å; and for $Cu_3Bi(SeO_3)_2O_2Br$ $a = 6.377(5)$, $b = 9.681(11)$, and $c = 7.268(4)$ Å. These values are in good agreement with the previously reported ones [3,13]. No indications of the presence of secondary phases were detected. The magnetization, thermal conductivity, and specific heat measurements were performed using relevant options of the Quantum Design PPMS-9T device. The measurements of permittivity at the frequency $f = 2 \times 10^4$ Hz were done with the capacitance method using an Andeen-Hagerling 2700A bridge. The electric polarization measurements in $Cu_3Bi(SeO_3)_2O_2Cl$ in both the presence and absence of poling bias up to 170 kV/m were performed with the Sawyer-Tower method using a homemade setup. To create electrical contacts, the flat surfaces of the crystals were coated by Au-Ti films by means of magnetron sputtering. Freshly cleaved platelike samples with a size of about $3 \times 3 \times 1\,mm^3$ were used for the Raman scattering investigations. Experiments were performed in quasibackscattering geometry, using a $\lambda = 532$-nm solid-state laser. The laser power was set less than 2 mW with a spot diameter of about 100 μm to avoid heating effects. Raman spectra were measured in both parallel (XX, $X'X'$) and crossed (XY, $X'Y'$) polarizations, with light polarized in the basal ab plane. The measurements were carried out in a closed-cycle cryostat, Oxford/Cryomech Optistat, in the temperature range from 8 to 295 K. The spectra were collected via a triple spectrometer Dilor-XY-500 by a liquid nitrogen cooled charge-coupled device (CCD) Horiba Jobin Yvon, Spectrum One CCD-3000V.

B. Bulk properties

Magnetic properties of $Cu_3Bi(SeO_3)_2O_2X$ (not shown) were found to be in full correspondence with earlier published data [5,12,14] with sharp transitions to the antiferromagnetically ordered state at comparable Néel temperatures T_N. At $T < T_N$, both compounds exhibit pronounced magnetic anisotropy and sharp field-induced metamagnetic phase transitions.

The specific heat measurements C vs T, shown in Fig. 2, confirm the formation of long-range magnetic order in $Cu_3Bi(SeO_3)_2O_2X$ marked by sharp λ-type anomalies at $T_N \sim 25$ K with Néel temperature in the Br compound being slightly higher compared to the Cl compound. An additional anomaly at $T^* \sim 115$ K is seen in the temperature dependence of the specific heat in the Cl compound. This anomaly, not observed in magnetic properties, is ascribed to the structural phase transition. The measurements of dielectric permittivity in $Cu_3Bi(SeO_3)_2O_2X$, shown in the inset of Fig. 2, further confirm structural phase transition in $Cu_3Bi(SeO_3)_2O_2Cl$ at

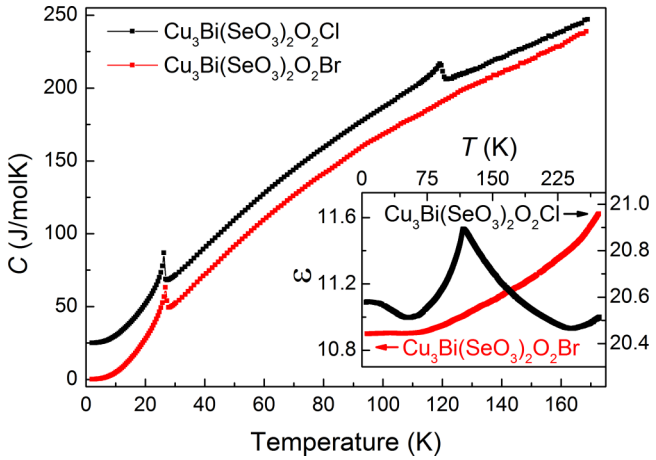

FIG. 2. Specific heat C of $Cu_3Bi(SeO_3)_2O_2X$ single crystals as a function of temperature. The inset represents the temperature dependences of dielectric permittivity ε taken at cooling at the frequency $f = 20$ kHz.

T^*. Both specific heat and dielectric permittivity anomalies are continuous, being consistent with the second-order transition scenario. The anomalous behavior spreads over a wide temperature range while the magnitude of the anomaly $\Delta\varepsilon/\varepsilon \sim 2\%$ is very small. Similarly small is the spread of polarization loop P vs E detected in both the presence and absence of a poling bias, as shown in Fig. 3. The shape of the loop, distinctly different from that expected for antiferroelectric phase, indicates the presence of the polar phase inclusions in the sample.

The temperature dependence of thermal conductivity κ, shown in Fig. 4, reveals anomalous behavior of this parameter at $T > T^*$, i.e., κ decreasing upon lowering the temperature. This type of behavior reflects the lattice instability when approaching the structural phase transition [22]. In a way, these data support the observations that the shortened Cu2-Cl

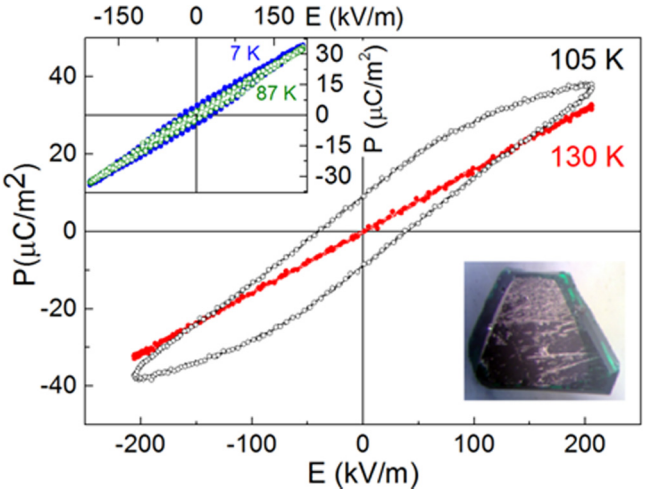

FIG. 3. The electric polarization loops taken both above and below the structural transition temperature $T^* \sim 115$ K in the single crystal of $Cu_3Bi(SeO_3)_2O_2Cl$ at $E_{gate} = 170$ kV/m. The upper inset represents the polarization loops obtained at $T < T^*$ at no gating voltage. The lower inset is the photograph of an Au-Ti coated sample with the c axis oriented perpendicular to the plate.

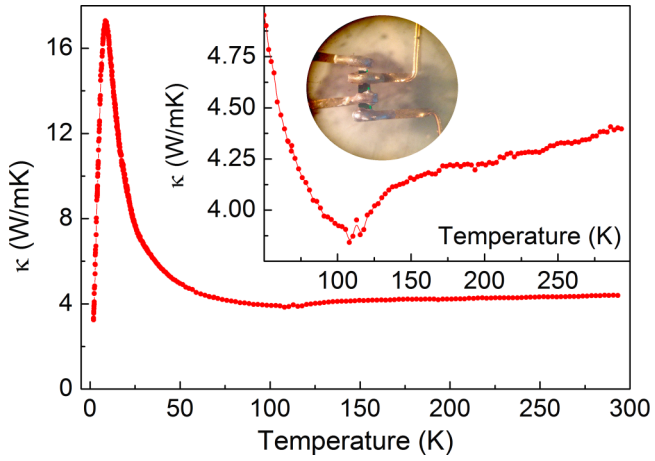

FIG. 4. The temperature dependence of thermal conductivity in $Cu_3Bi(SeO_3)_2O_2Cl$. The inset represents an enlarged view of $\kappa(T)$ dependence in the vicinity of T^* and the photograph of the sample mount.

distances in the structure of $Cu_3Bi(SeO_3)_2O_2Cl$ are already formed at high temperatures [3]. The phase transition at T^* is marked by the pronounced minimum in thermal conductivity; some instability is evident in the vicinity of this temperature. Below T^*, κ follows the behavior expected for the phonon-mediated thermal conductivity. Initially, κ rises due to the increase in the phonon's mean free path, reaches the so-called phonon peak at $T_{ph} = 8.5$ K, and rapidly decreases due to depletion of the phonon population. No signatures of magnetic phase transition at $T_N \sim 25$ K are detected in thermal conductivity measurements.

C. Lattice vibrations

The factor group analysis for the centrosymmetric *Pmmn* space group yields 78 active and nine silent optical modes:

$$\Gamma^{\text{optical}} = 12A_g^R + 6B_{1g}^R + 9B_{2g}^R + 12B_{3g}^R + 14B_{1u}^{IR} + 14B_{2u}^{IR} + 11B_{3u}^{IR} + 9A_{1u},$$

where the superscript R and IR stand for Raman- and infrared-active modes, respectively. The corresponding Raman tensors are given by the following matrices:

$$A_g = \begin{pmatrix} a & 0 & 0 \\ 0 & b & 0 \\ 0 & 0 & c \end{pmatrix}, \quad B_{1g} = \begin{pmatrix} 0 & d & 0 \\ d & 0 & 0 \\ 0 & 0 & 0 \end{pmatrix},$$

$$B_{2g} = \begin{pmatrix} 0 & 0 & e \\ 0 & 0 & 0 \\ e & 0 & 0 \end{pmatrix}, \quad B_{3g} = \begin{pmatrix} 0 & 0 & 0 \\ 0 & 0 & f \\ 0 & f & 0 \end{pmatrix}.$$

At room temperature, 18 and 17 $A_g + B_{1g}$ phonon modes are identified in $Cu_3Bi(SeO_3)_2O_2Br$ and $Cu_3Bi(SeO_3)_2O_2Cl$, respectively. This agrees with the expected 18 Raman-active phonons. The narrow line shape of the phonon lines, as shown in Fig. 5, provides additional evidence for the high quality of single crystals. The spectra are well polarized and the symmetry of each phonon mode can be easily defined.

Most experiments were carried out using $X'X'$ and $Y'X'$ scattering geometries with the sample rotated by some angle

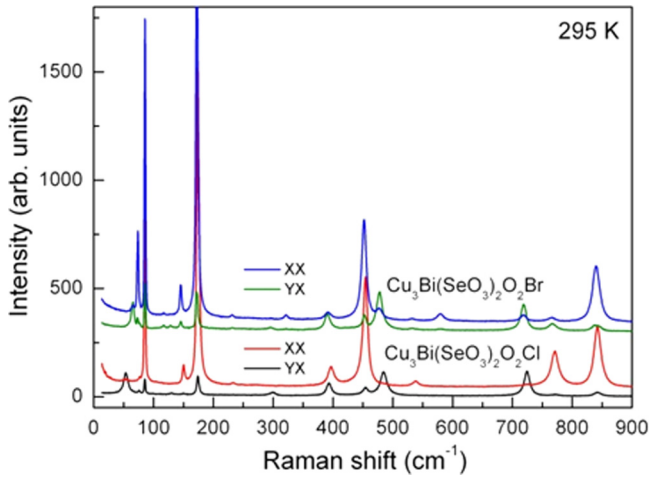

FIG. 5. The room-temperature Raman spectra of single crystals of $Cu_3Bi(SeO_3)_2O_2X$ measured in both parallel XX and crossed XY polarizations, with light polarized in the ab plane.

with respect to the c axis. The appropriate Raman tensors for the scattering from the ab plane are given by the following matrices:

$$A_g = \begin{pmatrix} a' & d' & 0 \\ d' & b' & 0 \\ 0 & 0 & c \end{pmatrix}, \quad B_{1g} = \begin{pmatrix} e' & f' & 0 \\ f' & -e' & 0 \\ 0 & 0 & 0 \end{pmatrix}.$$

Therefore, in any scattering polarization, say $X'X'$, all A_g and B_{1g} excitations will be present in the experimental spectrum. Note that the spectra may also contain weak peaks of B_{2g} and B_{3g} symmetry leaking from forbidden polarizations due to the wide aperture of collecting spectrometer optics.

The Raman spectra at selected temperatures are shown in Fig. 6. At room temperature, the high-frequency parts of the spectra of Br and Cl compounds are identical, reflecting isostructural similarity of both compounds. Below T^*, a number of new phonon modes appears in the Raman spectra of the Cl compound as listed in Table I. The significantly richer low-frequency part of the spectra in

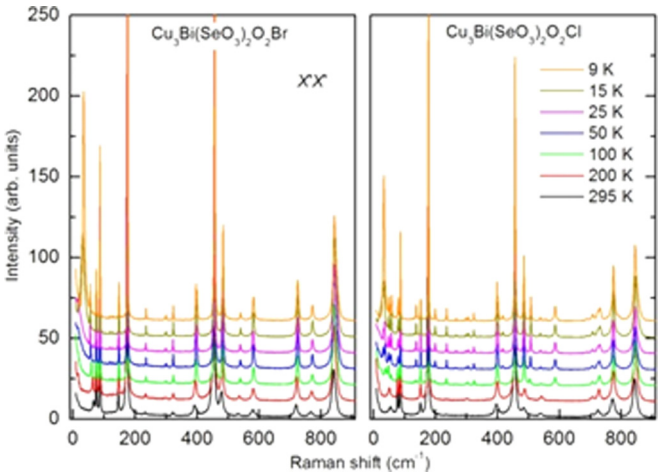

FIG. 6. The temperature-dependent $X'X'$ Raman spectra in $Cu_3Bi(SeO_3)_2O_2X$.

TABLE I. The modes seen in $Cu_3Bi(SeO_3)_2O_2X$ Raman spectra at selected temperatures. The lines appearing at $T < T^*$ in $Cu_3Bi(SeO_3)_2O_2Cl$ are marked with an asterisk (*).

Raman frequencies (cm^{-1})				
X = Cl				X = Br
9 K		100 K	295 K	295 K
A_g	B_{1g}	$A_g + B_{1g}$	$A_g + B_{1g}$	$A_g + B_{1g}$
31.1*		24.5*		
	33.6*	37.8*		
38.3*		40.8*		
	48.6	48.1	54.8	65.1
57.8*	55.6*	55.9*		
78.2	78.1	77.0	77.4	74.1
81.4*		80.6*		
86.2		86.4	86.3	86.1
	119.7*	120.2*		117.4
	130.8	131.1	130.5	129.6
137.5*		137.1*		
150.2		151.8	151.0	145.9
151.6				
176.8		176.8	175.1	172.9
	189.2*	189.0*		
198.0*		197.6*		
200.4*		200.5*		
235.3		235.4	233.0	232
	266.4*	266.8*		
	297.8*	298.7*		
	305.6	304.4	299.0	296.6
322.5*		324.1*		322
347.5*		347.5*		
	397.5	397.6	396.3	391.9
400.8		401.6		
417.2*		416.2*		
455.9		456.9	455.0	452.2
	484.7	486.2	485	478.3
	507.1*	504.3*		
537.5		540.8	538.6	533
555.5*		552.1*		
586.0*		585.8*	583.4*	580.2
689.0*		688.0*		
	723.7	724.0	724.7	719.1
	730.2*	729.0*		
774.2		774.2	771.2	766.9
844.3		844.8	842.4	840.6

$Cu_3Bi(SeO_3)_2O_2Cl$ reflects its reduced symmetry as compared to $Cu_3Bi(SeO_3)_2O_2Br$.

The temperature dependences of frequency, linewidth, and intensity of two representative phonons with similar energies in $Cu_3Bi(SeO_3)_2O_2X$ (X = Br, Cl) are compared in Fig. 7. The phonon mode of A_g symmetry at $\sim$450 cm^{-1} shows a behaviour expected for anharmonicity and thermal expansion effects. Both structural and magnetic phase transitions in the

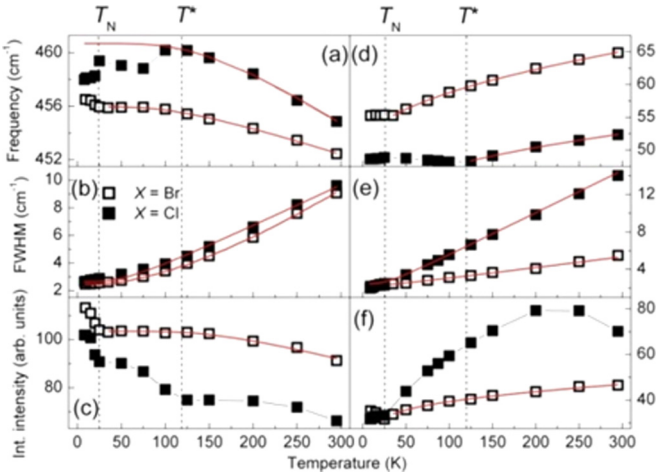

FIG. 7. The parameters of two representative phonon modes in $Cu_3Bi(SeO_3)_2O_2Br$ (open symbols) and $Cu_3Bi(SeO_3)_2O_2Cl$ (closed symbols). The (a,d) panels refer to frequency, the (b,e) panels refer to linewidth (FWHM), and the (c,f) panels refer to integrated intensity of the B_{1g} and A_g phonon modes, respectively.

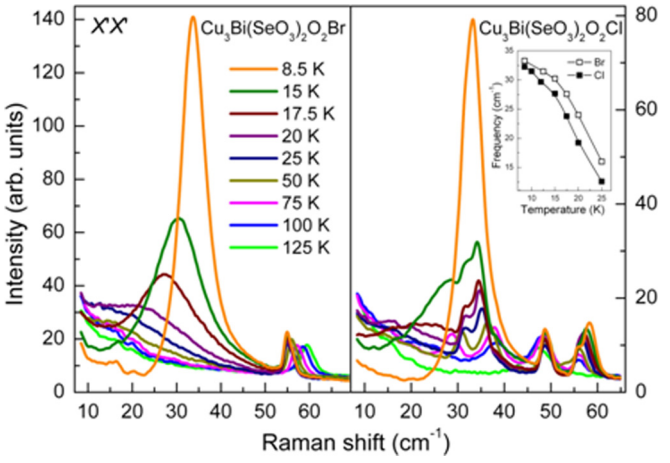

FIG. 8. The low-frequency Raman spectra in $Cu_3Bi(SeO_3)_2O_2X$ at selected temperatures. The inset represents the temperature dependences of the magnon peak in both the Cl and Br compounds.

Cl compound are accompanied by the softening of this mode. Magnetic order has the opposite action on the phonon's energy in the Br compound, which deserves further investigation. The lattice instability of both compounds is indicated by the behaviour of the phonon mode of B_{1g} symmetry at $\sim$55 cm^{-1}, which shows systematic energy reduction upon lowering the temperature. This conclusion is also supported by the characteristic decrease of the B_{1g} mode intensity. Note that the B_{1g} phonon linewidth in $Cu_3Bi(SeO_3)_2O_2Cl$ is twice as large compared to $Cu_3Bi(SeO_3)_2O_2Br$, signaling stronger lattice fluctuations in the former compound.

D. Magnetic excitations

Below T_N, an additional low-frequency signal appears in both $Cu_3Bi(SeO_3)_2O_2Br$ and $Cu_3Bi(SeO_3)_2O_2X$Cl suggesting its purely magnetic origin and insensitivity to structural distortions observed in the Cl compound at T^*. At low temperatures, the intensity of the magnon line exceeds the intensities of the neighboring phonons by an order of magnitude, as shown in Fig. 8. The temperature dependences of the frequency of these lines are shown in the inset to the right panel of Fig. 8. At the lowest temperatures, the energy of this mode 33.5 cm^{-1} compares favorably with both the magnon's excitation observed with infrared spectroscopy [12], and the spin gap found recently in inelastic neutron scattering measurements in the Cl compound [4]. The asymmetric shape of the magnon mode is in accord with the presumption of the spin gap origin of this line. The magnon mode strongly overlaps with several low-frequency phonon lines in the Cl compound while this effect is absent in the Br compound.

III. DISCUSSION

The Raman spectra of $Cu_3Bi(SeO_3)_2O_2X$ are similar at room temperature, being well described with the nonpolar *Pmmn* structure. Upon lowering the temperature, no qualitative changes in the spectra are seen in the Br compound. At the same time, the numerous new lines seen in the Cl compound at $T < T^*$ signify structural phase transition. The crystal structures suggested for the low-temperature phase of $Cu_3Bi(SeO_3)_2O_2Cl$ differ mainly in the displacement pattern of Cl and Cu2 ions. Both $P2_1mn$ and *Pcmn* phases have the same intralayer electric dipole moment composed of out-of-phase shifts of the Cl and Cu2 ions along the *a* axis. In the *Pcmn* phase the intralayer electric dipole moments are stacked in the opposite direction on adjacent layers, which leads to the primitive cell doubling along the *c* axis. The Raman data obtained could be equally well described in both $P2_1mn$ and *Pcmn* space groups. However, the observation of superstructure peaks pertinent for the *Pcmn* phase with doubled *c* parameter [3,5] defines the symmetry of the low-temperature phase unambiguously as a nonpolar one. Thus, structural transition involves a distortion from the centrosymmetric *Pmmn* phase to the centrosymmetric *Pcmn* phase.

Regarding bulk properties, the *Pcmn* structure is a nonpolar antiferroelectric phase while the $P2_1mn$ structure is a polar ferroelectric one. The polarization loops for ferroelectric and antiferroelectric dipole arrangements differ qualitatively. Our measurements of the polarization loop in $Cu_3Bi(SeO_3)_2O_2Cl$ at $T < T^*$ identify a ferroelectric response in both the absence and presence of a poling bias. In the former case, the loop appears due to domain boundaries' motion and repolarization of ferroelectric domains. In the latter case, the application of a poling bias just reveals the intrinsic properties of a ferroelectric phase.

It should be noted, however, that the observed ferroelectric response is matched to the geometry of the experiment, which measures the dielectric response along the *c* axis. For the $P2_1mn$ structure the electric polarization should develop along the *a* axis in accordance with Cl and Cu2 displacements shown in Fig. 1. Besides, the ferroelectric response was found to be orders of magnitude lower as compared to known ferroelectric phases. These observations lead us to conclude that minor inclusions of the ferroelectric phase randomly oriented within the matrix of the major antiferroelectric phase are present in

the low-temperature state of the $Cu_3Bi(SeO_3)_2O_2Cl$ samples investigated.

IV. CONCLUSION

In the present work, we performed a detailed Raman study of the temperature dependences of vibrational and magnetic excitations in $Cu_3Bi(SeO_3)_2O_2X$ (X = Cl, Br) single crystals. During our studies we detected a second-order structural phase transition at $T^* \sim 115$ K in $Cu_3Bi(SeO_3)_2O_2Cl$ accompanied by the appearance of new phonon modes while no structural changes were detected in the Br compound. The temperature dependences of specific heat C, thermal conductivity κ, and dielectric permittivity ε confirm these observations. At $T < T^*$, the electric polarization loop at $P \parallel c$ axis under both the presence and absence of a poling bias signals the presence of weak ferroelectricity. The magnetic phase transitions at $T_N \sim 25$ K are marked by sharp λ-type singularities in both compounds. At $T < T_N$, a low-frequency, highly intensive scattering signal of magnetic origin is observed in both Cl and Br compounds being virtually insensitive to structural phase transition. At the lowest temperatures, the energy of this mode compares favourably with both the magnon excitation observed in infrared spectroscopy [18] and the global spin gap found in inelastic neutron scattering measurements in the Cl compound [4].

ACKNOWLEDGMENTS

We acknowledge valuable discussions with A. Tsirlin, V. G. Mazurenko, and J.-Y. Lin. This work was supported by the Ministry of Education and Science of the Russian Federation in the framework of the Increase Competitiveness Program of NUST "MISiS" No. K2-2016-066 and by Act 211 of the Government of the Russian Federation, Agreements No. 02.A03.21.0004 and No. 02.A03.21.0011. This work was also supported by the NTH-School "Contacts in Nanosystems: Interactions, Control and Quantum Dynamics", the Braunschweig International Graduate School of Metrology (IGSM), and DFG-RTG 1952/1, Metrology for Complex Nanosystems.

[1] I. Rousochatzakis, J. Richter, R. Zinke, and A. A. Tsirlin, Phys. Rev. B **91**, 024416 (2015).
[2] S. A. Nikolaev, V. V. Mazurenko, A. A. Tsirlin, and V. G. Mazurenko, Phys. Rev. B **94**, 144412 (2016).
[3] D. A. Prishchenko, A. A. Tsirlin, V. Tsurkan, A. Loidl, A. Jesche, and V. G. Mazurenko, Phys. Rev. B **95**, 064102 (2017).
[4] E. Constable, S. Raymond, S. Petit, E. Ressouche, F. Bourdarot, J. Debray, M. Josse, O. Fabelo, H. Berger, S. deBrion, and V. Simonet, Phys. Rev. B **96**, 014413 (2017).
[5] H. C. Wu, K. D. Chandrasekhar, J. K. Yuan, J. R. Huang, J.-Y. Lin, H. Berger, and H. D. Yang, Phys. Rev. B **95**, 125121 (2017).
[6] M. Pregelj, O. Zaharko, A. Zorko, M. Gomilšek, O. Sendetskyi, A. Gunther, M. Ozerov, S. A. Zvyagin, H. Luetkens, C. Baines, V. Tsurkan, and A. Loidl, Adv. Funct. Mater. **25**, 3634 (2015).
[7] A. Zorko, M. Gomilšek, M. Pregelj, M. Ozerov, S. A. Zvyagin, A. Ozarowski, V. Tsurkan, A. Loidl, and O. Zaharko, AIP Adv. **6**, 056210 (2016).
[8] A. Pring, B. M. Gatehouse, and W. D. Birch, Am. Mineral. **75**, 1421 (1990).
[9] P. S. Berdonosov and V. A. Dolgikh, Russ. J. Inorg. Chem. **53**, 1353 (2008).
[10] R. Becker and M. Johnsson, Solid State Sci. **7**, 375 (2005).
[11] S. R. J. Oliver, Chem. Soc. Rev. **38**, 1868 (2009).
[12] K. H. Miller, P. W. Stephens, C. Martin, E. Constable, R. A. Lewis, H. Berger, G. L. Carr, and D. B. Tanner, Phys. Rev. B **86**, 174104 (2012).
[13] P. Millet, B. Bastide, V. Pashchenko, S. Gnatchenko, V. Gapon, Y. Ksarid, and A. Stepanov, J. Mater. Chem. **11**, 1152 (2001).
[14] M. Pregelj, O. Zaharko, A. Günther, A. Loidl, V. Tsurkan, and S. Guerrero, Phys. Rev. B **86**, 144409 (2012).
[15] K. V. Zakharov, E. A. Zvereva, E. S. Kuznetsova, P. S. Berdonosov, V. A. Dolgikh, M. M. Markina, A. V. Olenev, A. A. Shakin, O. S. Volkova, and A. N. Vasiliev, J. Alloy Compd. **685**, 442 (2016).
[16] M. M. Markina, K. V. Zakharov, E. A. Zvereva, R. S. Denisob, P. S. Berdonosov, V. A. Dolgikh, E. S. Kuznetsova, A. V. Olenev, and A. N. Vasiliev, Phys. Chem. Miner. **44**, 277 (2017).
[17] K. V. Zakharov, E. A. Zvereva, P. S. Berdonosov, E. S. Kuznetsova, V. A. Dolgikh, L. Clark, C. Black, P. Lightfoot, W. Kockelmann, Z. V. Pchelkina, S. V. Streltsov, O. S. Volkova, and A. N. Vasiliev, Phys. Rev. B **90**, 214417 (2014).
[18] H. C. Wu, W. J. Tseng, P. Y. Yang, K. D. Chadrasekhar, H. Berger, and H. D. Yang, J. Phys. D: Appl. Phys. **50**, 265002 (2017).
[19] K. V. Zakharov, E. A. Zvereva, M. M. Markina, M. I. Stratan, E. S. Kuznetsova, S. F. Dunaev, P. S. Berdonosov, V. A. Dolgikh, A. V. Olenev, S. A. Klimin, L. S. Mazaev, M. A. Kashchenko, M. A. Ahmed, A. Banerjee, S. Bandyopadhyay, A. Iqbal, B. Rahaman, T. Saha-Dasgupta, and A. N. Vasiliev, Phys. Rev. B **94**, 054401 (2016).
[20] E. V. Nazarchuk, S. V. Krivovichev, O. Y. Pankratova, and S. K. Filatov, Phys. Chem. Miner. **27**, 440 (2000).
[21] See Supplemental Material at http://link.aps.org/supplemental/10.1103/PhysRevB.96.115144 for the crystal growth is described.
[22] A. N. Vasil'ev, V. V. Pryadun, D. I. Khomskii, G. Dhalenne, A. Revcolevschi, M. Isobe, and Y. Ueda, Phys. Rev. Lett. **81**, 1949 (1998).